nature communications

Article

https://doi.org/10.1038/s41467-025-60623-6

Flavoproteins as native and genetically encoded spin probes for *in cell* ESR spectroscopy

Received: 18 December 2024

Accepted: 29 May 2025

Published online: 01 July 2025

Check for updates

Timothée Chauviré[1,2], Siddarth Chandrasekaran[1], Robert Dunleavy[1], Jack H. Freed[1,2] & Brian R. Crane[1,2]

Flavin cofactors are attractive Electron Spin Resonance (ESR) probes for proteins because cellular reductants and light can generate their semiquinone states. Here, we use ESR spectroscopy to study the bacterial transmembrane aerotaxis receptor (Aer) in its native *Escherichia coli* membrane environment. Optimization of the spectroscopic (electronic relaxation times) and cell growth (isotopic labeling) conditions allow for measurements of Aer with its partners - the histidine kinase (CheA) and the coupling protein (CheW) - in native signaling arrays. Continuous-wave ESR measurements at room temperature show a rigid Aer flavin immobilized in the cofactor pocket and Q-band electron nuclear double resonance (ENDOR) measurements identify a predominant anionic semiquinone radical state *in cell*. Q-band four-pulse double electron-electron resonance (4P-DEER) measurements indicate a 4.1 nm distance between the two flavins of an Aer homodimer, consistent with previous in vitro measurements, but also reveal additional separations *in cell* indicative of chemoreceptor arrays, not previously observed for Aer. For general application, we further develop a genetically encoded Light-Oxygen and Voltage (LOV) domain for incorporation into target proteins as an ESR probe of structural properties *in cell*. This approach provides a framework to elucidate protein oligomeric states and conformations that are difficult to reproduce in vitro.

Flavins constitute redox-active protein cofactors that participate in a wide range of functions, including catalysis[1], light sensing[2], and signal transduction[3]. In fact, flavoprotein genes constitute between 1 and 3 percent of both prokaryote and eukaryote genomes[4,5]. The ability to undergo one- and two-proton-coupled electron transfer reactions provides versatility in enzymatic catalysis and allows for a diverse range of functions, including oxidoreductase, transferase, and lyase activities[6]. Flavoproteins also comprise major classes of blue-light photoreceptors in the form of cryptochromes, Light Oxygen Voltage (LOV) domains and Blue-Light using FAD (BLUF) domains, which sense and respond to environmental input in many different organisms[7]. Similarly, flavoproteins play a major role in signaling pathways, particularly in bacterial systems, where flavin-bound LOV and Per-Arnt-Sim (PAS) domains regulate kinase activity, DNA binding, and enzymatic activity[8]. This diversity of reactivity makes flavoproteins indispensable for a broad range of physiological functions, including oxidative damage response[9], small-molecule metabolism[1], and circadian rhythms[10].

The term flavin is used to describe compounds containing 7,8-dimethyl-10-alkylisoalloxazine, which are characteristically yellow in color. Flavin cofactors are usually found either as the flavin adenine dinucleotide (FAD) or the flavin mononucleotide (FMN), which are

[1]Department of Chemistry and Chemical Biology, Cornell University, Ithaca, NY, USA. [2]National Biomedical Center for Advanced ESR Technologies (ACERT), Cornell University, Ithaca, NY, USA. e-mail: bc69@cornell.edu

both metabolites of riboflavin (Vitamin B2) and differ by the R group attached to the N(10) atom[6]. The majority of flavoproteins (75%) utilize FAD as a cofactor, whereas the remaining (25%) utilize FMN[6]. Only a few proteins directly use riboflavin as a cofactor; for example, the sodium-pumping NADH:ubiquinone oxidoreductases of certain pathogenic bacteria, such as *Vibrio cholerae*[11].

Flavins assume three different redox states, the quinone (oxidized), semiquinone (one-electron reduction), and hydroquinone (two-electron reduction). Depending on the cofactor environment, the semiquinone state is encountered in two different protonation states: the neutral or the anionic semiquinone (NSQ or ASQ, respectively). In solution, the semiquinone state of free flavin is unstable and is rapidly reduced to the hydroquinone[12]. However, flavoproteins stabilize either the neutral or anionic semiquinone state, enabling both photochemical and catalytic properties distinct from the free cofactor[13].

The semiquinone state with its unpaired electron allows study by electron spin resonance (ESR) spectroscopy, which has been accomplished on both natural and synthetic semiquinones[13,14]. Because of their instability in aqueous solution, flavin semiquinone radicals have mostly been studied as protein-bound cofactors[13], although an agarose gel matrix has been used to stabilize the FMN semiquinone state, allowing stable radicals for days under aerobic conditions[15]. Protein-bound flavin semiquinones ranging from glucose oxidase[16] to light-sensing cryptochromes[17] have been analyzed using a combination of continuous wave ESR (cw-ESR) and pulsed ESR spectroscopy: pulsed dipolar spectroscopy (PDS), electron nuclear double resonance (ENDOR) or electron spin echo envelope modulation (ESEEM). Flavin semiquinones display characteristically broad features at X-band cw-ESR, with a linewidth of 1.5 mT for ASQs and 1.8–2.0 mT for NSQ due to inhomogeneous broadening from nitrogen and proton hyperfine interactions. Higher frequencies have been employed to accurately resolve g-factor tensor values using cw-ESR[16]. Pulsed ENDOR methods, such as Davies ENDOR, are particularly valuable to measure the large hyperfine couplings of flavin semiquinones[18]. In addition, three and four-pulse ESEEM methods have been used to characterize hyperfine coupling constants (hfccs) in select flavoproteins[19].

We sought to investigate the use of flavin semiquinone radicals for *in cell* measurement with ESR spectroscopy. Flavin cofactors offer several advantages for this application as they are tightly bound in their cofactor pocket, with dissociation constants in the nanomolar range[20]. Flavin binding domains are also small enough to be attached to the termini of a protein of interest; for example, FMN-binding LOV domains average only 110 residues[21]. Because FAD and FMN are natural metabolic cofactors, the addition of exogenous cofactors is unnecessary for protein expression. The formation of ASQ or NSQ radicals can be induced by either chemical reductants or through illumination with blue light (λ = 420–480 nm), as some flavoproteins readily undergo flavin photoreduction. For *in-cell* measurements, reduction can be accomplished in the reducing environment of the cell for certain proteins and enhanced by light.

Aer is an FAD-containing transmembrane protein in *E. coli* responsible for movement towards environments rich in terminal acceptors of the electron-transport chain, such as oxygen under aerobic conditions (i.e., aerotaxis)[22]. Aer is an obligate homodimer with multiple domains, an N-terminal FAD-binding PAS domain, a two-helix transmembrane region (per subunit), a HAMP signaling domain (histidine kinases, adenylyl cyclases, methyl-accepting chemotaxis proteins, phosphatases), and a C-terminal kinase control domain[22] (Fig. 1a, b). Aer indirectly senses oxygen by measuring the redox environment of the cell through reactivity of its FAD-bound cofactor[23–26]. Changes in the FAD redox state induce conformational changes to the cytoplasmic kinase control domain, which in turn regulates activity of the histidine kinase CheA[27]. CheA phosphorylates a response regulator (CheY), which binds to the flagellar motor and switches the sense of motor rotation. Oxidized FAD in Aer supports CheA activation, whereas reduction to the anionic semiquinone inhibits CheA[28]. Physiological experiments suggest a third, hydroquinone form of FAD also producing CheA activation[23], but the reduced hydroquinone state is not stable in purified Aer under aerobic conditions[28]. Within cells, *E. coli* chemoreceptors that regulate CheA associate as trimers-of-dimers (TODs) and extended molecular arrays of hexagonal symmetry in the membrane[29–33]. The cytoplasmic HAMP and kinase-control regions of Aer are closely related to those of chemoreceptors, and Aer does appear to form higher-order oligomers in vitro[27]. Moreover, disulfide crosslinking patterns between engineered cysteine residues are consistent with Aer forming TODs in vivo[34]; however, it's unclear if these TODs form higher-order assemblies.

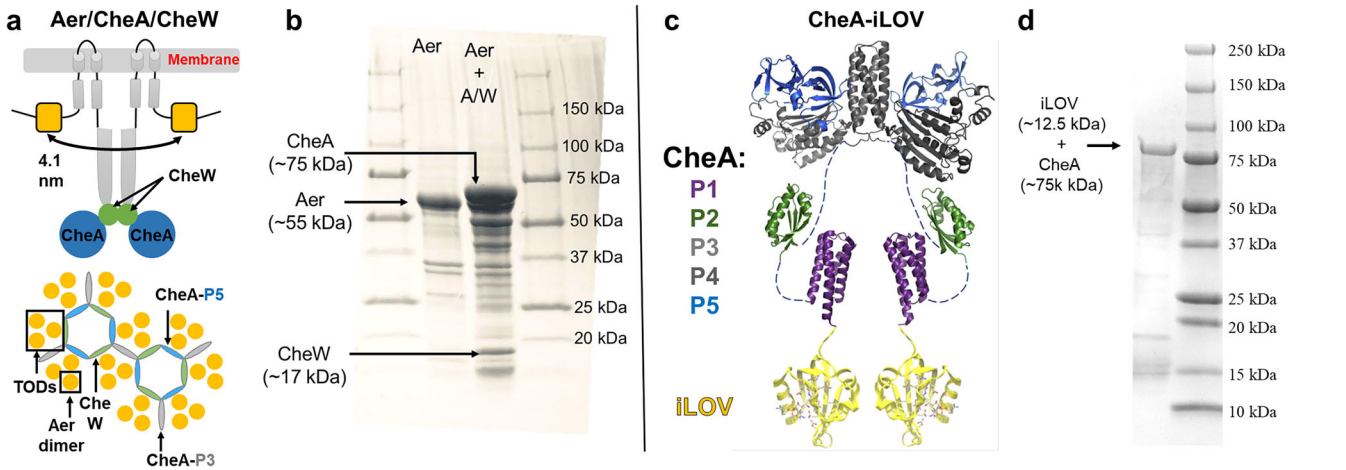

Fig. 1 | The two different chemosensory systems analyzed by Electron Spin Resonance: Aer with an endogenous flavin center and CheA with an extraneous flavin center supplied by a small flavoprotein iLOV. a Representation of Aer and its binding partners, CheA & CheW, on the inner membrane of *E. coli* as viewed parallel to the membrane (top) and as viewed normal to the membrane (bottom); CheW (green lines), and the P5 domain of CheA (blue lines) form hexameric rings that bind receptor trimers-of-dimers (TODs). Aer homodimers (yellow dots) assemble into TODs (boxed). Two TODs, one CheA dimer and two CheW proteins, compose a core complex, as bridged by the CheA dimerization domain P3 (gray line). **b** SDS-PAGE gel of the membrane fraction of BL21-DE3 cells overexpressing Aer (only) or Aer with CheA/CheW. **c** Representation of the fusion of the FMN-binding iLOV (~12.5 kDa) to the N-terminus of CheA (P1 Domain); the P1 domains of CheA are predicted to dimerize when incorporated into receptor arrays. **d** SDS-PAGE gel of the membrane fraction of BL21-DE3 cells overexpressing CheA-iLOV. Gels are representative of at least 3 biological replicates, see Supplementary Tables 3 and 9.

https://doi.org/10.1038/s41467-025-60623-6

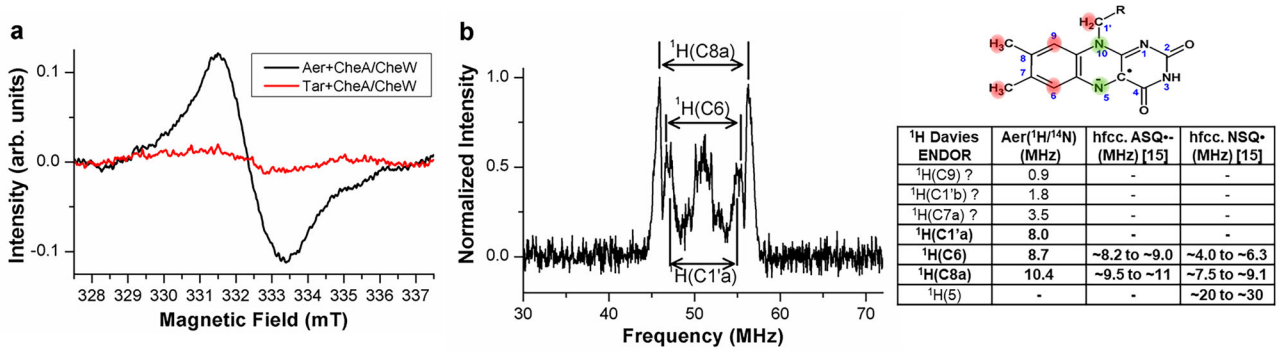

¹H Davies ENDOR	Aer(¹H/¹⁴N) (MHz)	hfcc. ASQ•⁻ (MHz) [15]	hfcc. NSQ• (MHz) [15]
¹H(C9) ?	0.9	-	-
¹H(C1'b) ?	1.8	-	-
¹H(C7a) ?	3.5	-	-
¹H(C1'a)	**8.0**	**-**	**-**
¹H(C6)	**8.7**	**~8.2 to ~9.0**	**~4.0 to ~6.3**
¹H(C8a)	**10.4**	**~9.5 to ~11**	**~7.5 to ~9.1**
¹H(5)	-	-	**~20 to ~30**

Fig. 2 | X-band continuous-wave Electron Spin Resonance (cw-ESR) and Q-Band Electron Nuclear Double Resonance (ENDOR) spectra of Aer *in cell*. **a** X-band cw-ESR spectra of BL21 (DE3) cells overexpressing CheA/CheW along with Aer (black curve) or Tar (red curve); (**b**) Q-band ^{1}H Davies ENDOR spectra of Aer co-expressed with CheA/CheW in BL21 (DE3) cells observed at $T = 150$ K; The structure of the flavin isoalloxazine ring with the flavin protons highlighted in red along with their corresponding ENDOR frequencies below. The ^{1}H hyperfine coupling constants (hfccs) (^{1}H(C8a), ^{1}H(C6) and ^{1}H(C1'a)) attribution was done by analogy to hfccs found in the literature[15,18], and their values are reported in the table inset.

We have previously used light-generated semiquinone radicals to determine the positioning of the Aer PAS sensing domains when full-length Aer was incorporated into nanodiscs[27]. Herein, we investigate the Aer receptor *in cell* both to provide native information about Aer and to elucidate general parameters for *in cell* flavoprotein ESR analysis. Previously, *in cell* ESR on flavoproteins performed for *Arabidopsis thaliana cryptochrome* 1 and 2 (cw-ESR, transient ESR and ENDOR)[18,35–39] and *Drosophila melanogaster* cryptochrome (X-band cw-ESR, ENDOR)[40], both in insect cells (Sf21) provided direct evidence of ASQ and NSQ formation, respectively, upon illumination with blue light[18,35–40]. In addition to cw-ESR and ENDOR, pulsed dipolar spectroscopy (PDS), such as four-pulse double electron-electron resonance (4 P-DEER), has the potential to directly report on native protein conformations within cells. This approach could be particularly advantageous if the environment and interaction partners of the protein of interest are unknown and/or difficult to reconstitute in vitro.

In cell PDS measurements are challenging for several reasons: (1) delivery of spin-labeled biomolecules into cells is generally difficult, (2) spin labels are usually unstable in the reducing environment of the cell, (3) the spin-spin relaxation time (T_2), also known as the phase memory time (T_m) of the spin label, is too short due to various relaxation pathways present in the crowded cellular environment. To date, a few types of paramagnetic species have been employed in PDS measurements *in cell*, these include nitroxide spin labels[41–48], gadolinium complexes[49–54], trityl derivatives[55–58], tyrosine radicals[59] and copper-NTA complexes[60,61]; however, to our knowledge, flavins have yet to be used as paramagnetic centers for *in cell* PDS measurements.

In this study, we show that both native flavoproteins and genetically engineered flavoprotein domains can be successfully used for *in cell* distance measurements. We investigate two systems involved in the *E. coli* chemotaxis signaling pathway: (1) the energy sensor Aer co-expressed with the scaffold protein CheW and the histidine kinase domain CheA (Fig. 1a,b), (2) the histidine kinase CheA fused with a small (12.5 kDa) engineered Light Oxygen Voltage (LOV) domain (Fig. 1c, d). Whole cell isotope labeling with ^{15}N and ^{2}H and temperature-dependent studies are employed in order to optimize relaxation properties for 4P-DEER measurements. Overall, these findings provide a template for further *in cell* studies of both native flavoproteins and flavoprotein-based probes.

Results and discussion

Continuous-Wave ESR and pulsed ENDOR of Aer *in cell*

The structural changes in Aer responsible for its energy taxis behavior are not fully understood, although considerable progress has been made[62]. Nonetheless, it is difficult to isolate and characterize functional Aer complexes in vitro. Isolation of Aer in detergents, nanodiscs and lipodiscs[27,28] yielded Aer in primarily a dimeric state, with only minor evidence for the TODs responsible for cooperative signaling in *E. coli*[63]. All of the experiments presented here used *E. coli* BL21 (DE3) cells as the host bacterial system. The *aer* gene was expressed from the T7 promoter of pET-28a plasmid, either alone or with its signaling partners CheA/CheW (Fig. 1b). After growth, a cell pellet was immediately harvested, inserted into an ESR capillary and studied by cw-ESR at room temperature to determine the concentration of semiquinone radical. The capillary was then flash-frozen to carry out pulsed ESR measurements.

We estimate the concentration of cells inside the capillary at ~ 2-3 nM (~ 1.4–1.8·10^{10} cells per 20 µL) (Supplementary Table 1). In these samples, the cells are tightly packed; assuming an *E. coli* cell volume of ~ 1 fL[64], the cells account for ~ 90–95% of the wet volume. Although the capillary used was open-ended, such high concentrations of respiring cells will deplete oxygen in minutes and produce an anaerobic environment. To verify this assumption, oximetry experiments were conducted with lithium phtalocyanine (LiPc) as an oxygen-sensitive ESR probe[65,66] (Supplementary Fig. 1). According to the LiPc peak-to-peak linewidth, an O_2 concentration below 2% was measured for cells in either log phase or stationary phase in the ESR capillaries. Thus, *in cell* ESR measurements are conducted under anaerobic conditions owing to cell respiration. Notably, Aer mediates energy taxis to oxygen in aerobic conditions, but also other terminal electron acceptors, such as nitrate and fumarate, under anaerobic conditions[24].

Cw-ESR of over-expressed Aer in intact *E. coli* cells produced a stable signal of a characteristic semiquinone radical (Fig. 2a), whereas the similar expression of the non-FAD binding aspartate receptor Tar revealed no such signal. The cytosol of *E. coli* is a reducing environment[67–69] with a redox potential of ~ − 260 mV. The Aer redox potential in reconstituted systems is slightly lower at − 290 mV[28]. Given that cellular redox state depends on cellular environment, metabolic conditions and is not generally at equilibrium[70], it was unclear what the majority redox state of the Aer flavin would be in the cell. These measurements revealed that the anionic semiquinone state predominates.

Proteomics studies have shown that *E. coli* BL21 (DE3) cells do not express the major protein components of chemotaxis (CheA, CheW, Tsr, Tar); however, low levels of the receptors Trg and Aer were detected[71]. Aer and Trg are minor chemoreceptors in *E. coli*, accounting for less than 3–5% of the total amount of chemoreceptors in a motile *E. coli* cell[72]. Accordingly, *E. coli* BL21 (DE3) cells grown without

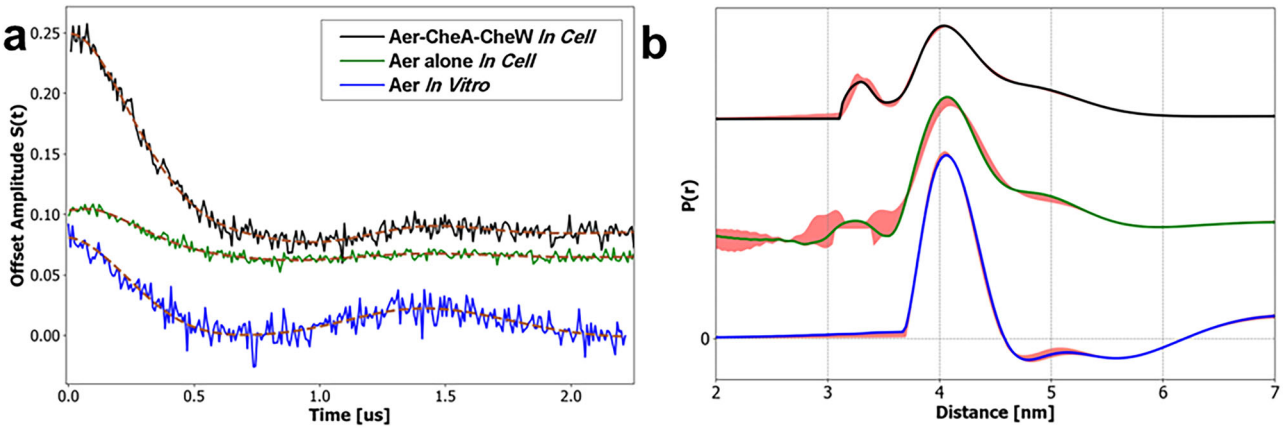

Fig. 3 | Four pulse double electron electron resonance (4P-DEER) spectra of Aer *in cell* at $T = 150$ K. a Time domain and (**b**) distance domain distribution between anionic semiquinone radicals of Aer in *E. coli* BL21 (DE3) cells co-expressed with CheA/CheW (black upper curve), of Aer alone in *E. coli* BL21 (DE3) cells (green middle curve), and of purified Aer solubilized in detergent (blue lower curve). The distance domain was obtained by using the SF-SVD method[117], and the time domain reconstructed spectrum is shown by a brown dashed line. Errors in the distance distributions represented by red shading was calculated as described in Srivastava et al.[117].

plasmid or with a plasmid containing CheA and CheW gave a residual cw-ESR signal of ~3 µM spin, which could be attributed to native Aer or other flavoproteins (Supplementary Fig. 2). Aer overexpression increased the concentration of semiquinone radical to 16 µM, whereas Aer overexpression with CheA and CheW produced a further increase to 26 µM. Earlier studies indicate that Aer expression leads to a concomitant overexpression of FAD[73,74], raising the possibility that a portion of the signal-producing FAD may have been unbound to Aer. However, FAD semiquinones (both ASQ and NSQ) rapidly decay in solution because of the presence of molecular oxygen and fast disproportionation reactions unless stabilized by a protein matrix[75,76]. Furthermore, experiments carried out on a variant of Aer (Tyr93His/Cys193His/Cys203His) with impaired flavin binding[73,77,78] showed a substantial reduction of the *in cell* semiquinone signal (Supplementary Fig. 3).

To further probe the radical state of Aer *in cell*, we performed Q-band ^{1}H Davies ENDOR measurements (Fig. 2b) at $T = 150$ K. The primary hfcc of 10.4 MHz corresponds to the H(8α) proton, whereas the hfccs observed at 8.7 and 8.0 MHz correspond to the ^{1}H(C6) and ^{1}H(C1′) protons, respectively. The relatively high value of ^{1}H(C8α)[18] and the absence of the large hfcc (~25 MHz) corresponding to ^{1}H(5) confirmed that Aer forms an ASQ radical *in cell*, as has been observed previously in preliminary overexpression experiments[28]. These values agree well with those from other ASQ-forming flavoproteins, including *Drosophila melanogaster* cryptochrome[17,40] and *Aspergillus niger* glucose oxidase[16].

Four-pulse DEER of Aer *in cell*

As Aer is presumed to form a homodimer in the cytoplasmic membrane[23,27], a 4.2 nm inter-subunit distance between flavin semiquinone radicals should be observed by 4P-DEER *in cell*. Indeed, 4P-DEER measurements for *in cell* Aer expressed alone, co-expressed with CheA/CheW, and in vitro Aer purified and solubilized in detergent (Supplementary Table 2) showed a similar distance at 4.1 nm (Fig. 3a, b). Thus, the cellular environment does not perturb the PAS domain positioning of the homodimer, and neither does association with CheA and CheW. The distance distribution for the radical pair is narrow with a width ranging from 0.2 to 0.3 nm (Full width half maximum (FWHM)), which indicates that the flavin is rigidly bound in the Aer PAS domain pocket on the nanosecond timescale of the experiment (Fig. 3b). Interestingly, additional distances (3.3 nm and 4.9 nm) were observed for Aer/CheA/CheW *in cell*. Whereas the 4.9 nm distance should be interpreted with caution (as the background subtraction used can interfere and lead to artefactual signals at longer distances[79–81]), the shorter distance indicated association of Aer dimers in the cell membrane. Such a short distance is unlikely to arise from a single dimer because the HAMP domains that separate the PAS domains prevent a flavin-to-flavin separation closer than 4.1 nm. Interestingly, the intensity of the shorter distance (compared to the intensity of the 4.1 nm homodimer distance) is considerably diminished when Aer is expressed without CheA/CheW (Supplementary Fig. 4), thereby indicating that the signaling partners stabilize assembly of Aer dimers into higher-order structures.

The time domain of the 4P-DEER spectrum can also be analyzed in terms of an intensity factor that is called modulation depth. The modulation depth, which reflects the number of spins experiencing dipolar interactions within the distance range of sensitivity, depends on several factors: the labeling efficiency[79,81]; the inversion efficiency of the pump pulse[79]; and the proportion of multimeric states[82,83]. The time domain 4P-DEER signal for Aer *in cell* when co-expressed with CheA/CheW (Fig. 3a) displayed a modulation depth of 15.7% (Supplementary Table 2), which is typical for flavin anionic semiquinone radicals at Q-band[84]. Overexpression of Aer in the absence of CheA/CheW caused a significant drop in the modulation depth (to 3.6%) (Supplementary Table 2). We carried out multiple measurements to confirm that this drop in modulation depth was significant (Supplementary Table 3). Overexpression of Aer without its binding partners (CheA/CheW) likely leads to protein aggregation and, therefore, incomplete incorporation into the inner membrane of *E. coli*. Indeed, when expressed with CheA/CheW[73], Aer was associated primarily in the membrane fraction (high-speed centrifugation fraction), but in the absence of CheA/CheW, Aer was also associated with inclusion bodies and cellular debris (low-speed centrifugation fraction)[27]. The minor contributions from additional apparent distances, when Aer is expressed alone, may derive from some TODs formation in the membrane as well as associations present in these aggregated states.

Isotopic labeling of Aer/CheA/CheW *in cell*

For any spin system, an understanding of the relaxation properties (T_1 and T_m) is essential for optimal ESR data acquisition. For example, the longest distance that can be measured by 4P-DEER is T_m limited[81]. Phase memory times (T_m) of flavin cofactors bound to proteins are relatively short (T_m ~ 2 µs), and given that the dipolar oscillation frequency is inversely proportional to the cube of the distance between

https://doi.org/10.1038/s41467-025-60623-6

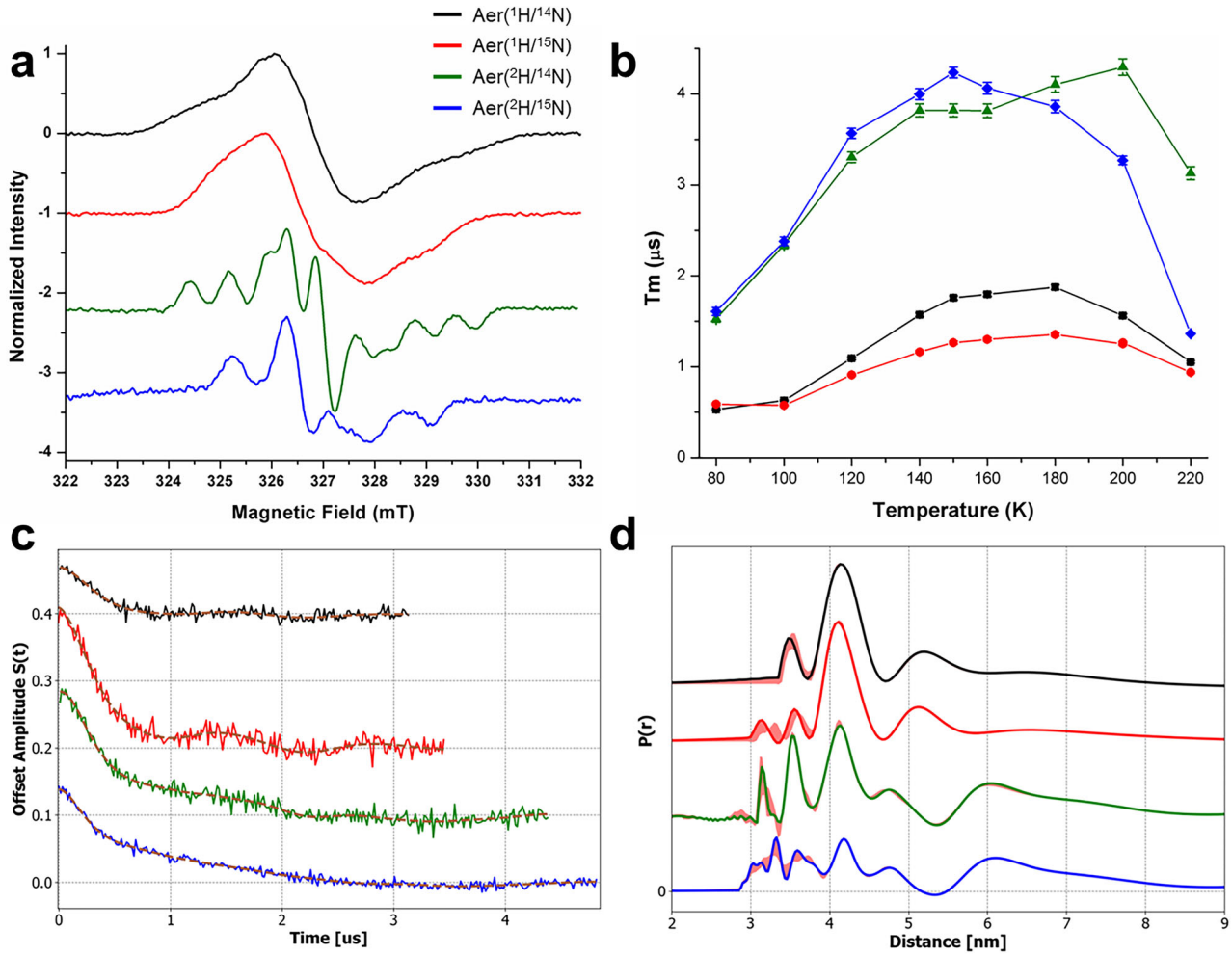

Fig. 4 | Continuous-wave Electron Spin Resonance (cw-ESR) and pulsed ESR analysis of Aer co-expressed with CheA/CheW in cells grown in different isotopically enriched media: in normal Luria Broth (LB) media (black curves), in $^{1}H/^{15}N$ Celtone media (red curves) in $^{2}H/^{14}N$ Celtone media (green curves) and in $^{2}H/^{15}N$ Celtone media (blue curves). a X-band *in cell* cw-ESR spectra of Aer/CheA/CheW measured at 293 K; (**b**) Phase memory relaxation time (T_m) measured by Q-Band two-pulse echo decay sequence. Each point represents the best value obtained by a monoexponential fit to the signal decay, and the error bars correspond to ± 2 · (standard deviations). The color symbol represents the following growth conditions: black square (normal LB media), red circle ($^{1}H/^{15}N$ Celtone media), green triangle ($^{2}H/^{14}N$ Celtone media) and blue diamond ($^{2}H/^{15}N$ Celtone media). **c** Time domain and reconstructed time domain (SF-SVD method[117]) (dashed brown line) measured at $T = 150$ K by Q-Band Four pulse double electron electron resonance (4P-DEER) sequence and (**d**) its associated distance distribution. Errors in the distance distributions represented by red shading was calculated as described in Srivastava et al.[117].

the spin labels, the maximum distance that can be measured is limited to ~ 5 nm[81]. Nonetheless, macromolecular complexes formed *in cell* can be separated by much larger distances (~10's of nm). Hence, lengthening the phase memory time of these flavin radicals will allow for measurements at longer evolution times.

Deuteration in the vicinity of the spin center substantially lowers the rate of spin relaxation. For the case of a nitroxide radical, deuterated buffer can increase spin relaxation times by a factor of ~ 2-3[85,86], whereas a fully deuterated protein can improve the relaxation properties of the radical by a factor of ~ 5[87]. Therefore, we explored if ^{2}H and ^{15}N labeling could improve the spin-relaxation properties of semiquinone radicals and resolve additional distances by 4P-DEER. To the best of our knowledge, no studies on the enhancement of spin relaxation by isotopic labeling have been conducted with flavin semiquinone radicals, particularly in cellular environments. Indeed, the effect of the reducing environment of the *E. coli* cytoplasm on spin relaxation properties is poorly understood. We expressed Aer/CheA/CheW in *E. coli* grown in three fully isotopically substituted media: ($^{2}H/^{14}N$), ($^{1}H/^{15}N$), and ($^{2}H/^{15}N$) and characterized the relaxation properties of the flavin ASQ. There was no difference in cell growth rate between $^{1}H/^{14}N$ and $^{1}H/^{15}N$ media. For ^{2}H media, cell doubling times were on the order of 2-3 h.

The cw-ESR spectra of Aer/CheA/CheW expressed in the four ($^{1}H/^{14}N$, $^{1}H/^{15}N$, $^{2}H/^{14}N$, $^{2}H/^{15}N$) isotopically defined media was immediately revealing (Fig. 4a). Under all labeling conditions, g-factors of 2.004 ± 0.001 (measured by comparison to a 2,2-diphenyl-1-picrylhydrazyl (DPPH) standard ($g_{DPPH} = 2.0036$)), were insensitive and in good agreement with previously reported g-factors for the semiquinone radical state in flavoproteins[13,88]. Relatively complex hyperfine interactions are expected for the flavin radical because the isoalloxazine ring contains multiple hydrogen and nitrogen atoms. However, these hyperfine peaks are typically not well resolved in $^{1}H/^{14}N$ and $^{1}H/^{15}N$ conditions due to the ESR linewidth. ENDOR experiments can help identify the ^{1}H hyperfine coupling interactions (Fig. 2b); nonetheless, the contributions of the nitrogen nuclei are usually obscured even in ENDOR. In the samples of Aer/CheA/CheW grown in deuterated media ($^{2}H/^{14}N$, $^{2}H/^{15}N$), the proton hyperfine interactions on the flavin ring were suppressed, and the nitrogen hyperfine interactions became

apparent. The cw-ESR spectra indicated that the underlying nitrogen hyperfine peaks can be attributed to two major nitrogen atoms - N5 and N10[14,89]. For the (^{2}H/^{14}N) Aer/CheA/CheW sample, we observed a characteristic nine-line cw-ESR spectra $(2 \times I + 1)(2 \times I + 1) = 9$, corresponding to the interaction of two non-equivalent ^{14}N atoms (I = 1). For the (^{2}H/^{15}N) Aer/CheA/CheW sample, we observed four-line spectra $(2 \times I + 1)(2 \times I + 1) = 4$ corresponding to the interaction of two non-equivalent ^{15}N nuclei (I = 1/2). The spectral lineshapes of the cw-ESR spectra were simulated using the EasySpin toolbox in MATLAB[90] with a consistent set of global parameters (Supplementary Fig. 5). In addition, hfccs (Supplementary Table 4) estimated for the two nitrogen atoms from 3P-ESEEM measurements carried out at Q-band (Supplementary Fig. 6) agree with the values obtained from cw-ESR measurements. These simulations were carried out in the rigid limit, and the best fit values (Supplementary Table 4) are close to the reported values for flavin radicals found by high-field ESR measurements[91] and for FMN radicals immobilized in an agarose matrix[15]. Our measurements confirmed that the flavin moieties are near the rigid limit and thus fixed within the protein pocket.

Next, we investigated the effect of isotopic modifications on the phase memory time T_m (Fig. 4b) and on the spin lattice relaxation time T_1 (Supplementary Fig. 7) of the flavin radical *in cell*. Earlier studies have characterized the temperature dependence on T_1 and T_m for related semiquinone radicals[92,93]. In particular, the presence of methyl groups on the isoalloxazine ring promotes additional spin relaxation at lower temperatures owing to the modulation of hyperfine interactions by their rotation. T_m for all of the samples followed the same trend of a bell-shaped[93–96] curve with a maximum between 150–180 K (Fig. 4b). Deuteration of the entire protein enhanced the T_m by a factor of ~3 at the T_m maxima whereas ^{15}N labeling produced only minor improvements. These bell-shaped curves derive from two phenomena: below 120 K, the magnetic inequivalence of hindered methyl protons (H7, H8) leads to additional cross-relaxation, whereas above 180 K, molecular motions increases and produces faster spin dephasing rates[97].

The spin lattice relaxation time T_1 decreased monotonically with the temperature, with values ranging from 0.2 ms (240 K) to values slightly greater than 1 ms at cryogenic temperatures (100 K and lower) for unlabeled Aer (^{1}H/^{14}N) (Supplementary Fig. 7). Isotopic replacement of ^{14}N with ^{15}N has marginal effects on T_1, whereas deuterium labeling enhanced the T_1 by a factor ~2–4, depending on the temperature. ^{2}H Mims ENDOR measurements confirmed deuterium substitution did not alter the flavin electronic structure (Supplementary Fig. 8 and Supplementary Table 5). Interestingly, unlike nitroxide spin labels[94], exchange of the protonated protein into a deuterated buffer alone does not enhance the spin relaxation of flavins significantly and no ^{2}H-ENDOR signal was detected in the sample exchanged with deuterated buffer (Supplementary Fig. 9). This lack of substitution likely confirms that the FAD cofactor, rigidly bound in the PAS domain of Aer, is inaccessible to the solvent.

Next, we performed 4P-DEER on the isotopically labeled *in cell* Aer/CheA/CheW sample, with the goal of probing longer distances with longer evolution times. Thus, isotopically labeled Aer/CheA/CheW ^{1}H/^{14}N, ^{1}H/^{15}N, ^{2}H/^{14}N and the ^{2}H/^{15}N samples were collected until 3.1, 3.5, 4.4 and 4.9 µs evolution times, respectively (Fig. 4c and Supplementary Table 6).

A clear dipolar oscillation is observed for all of the samples with a period of ~1.3 µs corresponding to the homodimer flavin separation of ~4.1 nm. (Fig. 4d). These results indicate that isotopic labeling did not significantly alter the arrangement of the PAS domains in Aer. Interestingly, additional distances from 3.2 nm to 6.5 nm were observed in all samples. Although these long distances have relatively higher uncertainty, even with 5 µs evolution times, separations in the 5–6.5 nm range do become accessible, which is not the case for T_m values of 2 µs. Moreover, the definition of the shorter distances also benefit from longer evolution times, which provide more periods of the higher frequency terms and a better background estimate. These additional distances *in cell* correspond with what would be expected for a TODs assembly state within a higher array organization[29–33,63]. Based on how other chemoreceptors associate into hexagonal arrays[29–33,63], we modeled an Aer oligomeric assembly (Fig. 5a) and revealed that the separation of the flavin centers in the assembly will only depend on a few parameters. The vertical position of the flavin relative to the membrane should be the same for each receptor due to the positioning of the transmembrane helices and known structures of the PAS domain[28]. Hence, the flavin separations will largely be determined in the 2 dimensions parallel to the membrane. Furthermore, the conserved interactions of CheW and CheA with the membrane-distal receptor tips should provide a similar TODs arrangement as observed for other receptor arrays[29–33,63,98]. Two trimers associate in what is defined as a core complex around one dimeric CheA[98,99], and then these core complexes can be extended into hexagonal arrangements by rings formed from CheA-P5 and CheW. The higher-order contacts between core complexes could also produce close distances among the flavin centers, but these interactions are somewhat uncertain as small changes at the CheA/CheW baseplate could propagate to much larger shifts at the level of the PAS domains, some 19 nm away. Nonetheless, the inter-dimer flavin distances will primarily depend upon the rotation angle of the flavin-to-flavin vector relative to a vector between the dimer center and the trimer center (α,β,γ, Fig. 5b,c). For example, with a fixed $\alpha = \beta = \gamma$ angle plane geometry (Supplementary Table 7), the distances of the *in cell* distributions of the isotopically labeled Aer/CheA/CheW (^{2}H/^{14}N) and (^{2}H/^{15}N) at 3.6 nm and 4.7 nm could arise from a TODs with fixed angles of ~120° (Supplementary Table 7 and Fig. 5a). A TODs with an angle of $\alpha = \beta = \gamma = 120°$ would induce two additional longer distances at 7.2 nm and 7.7 nm that could explain the large peaks observed in the 7 nm region. Nevertheless, this simple geometry model of a TODs fails to explain the 3.2-3.3 nm distance peaks.

We hypothesize that those peaks could derive from flavin-to-flavin distances that arise from two or more TODs (Fig. 5b). To explore this possibility, distances between every flavin (N_5 to N_5 distances) were cataloged in an array model that contained 2 core complexes (4 TODs) related by hexagonal symmetry. Distances larger than 8 nm were excluded because they would not be detected by pulse dipolar spectroscopy (Supplementary Table 8). A distance distribution was generated by summing single Gaussian curves for every distance with a standard deviation of 0.15 nm. The predicted distance distribution compared well to the experimental distance distribution obtained with the isotopically labeled Aer/CheA/CheW ^{2}H/^{15}N (Fig. 5d), with multiple distances around 3.2–3.6 nm and around 6-7 nm. No distances were observed below 3 nm due to the excluding radius of the PAS domain. We note that the 5.2 nm peaks observed in some spectrum, as well as the fine structure in the experimental distributions, could derive from other factors that include: a non-identical angle geometry ($\alpha \neq \beta \neq \chi$), a membrane curvature effect that alters planarity or conformational sampling, the latter due to heterogeneity of assembly or even the redox state of the Aer homodimer. Furthermore, the weighting of the distances in the model histogram will depend on the relative amounts of TODs, core complexes and larger assemblies *in cell*, factors that are difficult to predict.

Cysteine residues engineered into the periplasmic loops of the Aer transmembrane domains at positions 187 and 191 produce inter-dimer disulfide links, as does residue 379 in the cytoplasmic tip, which interacts with CheA and CheW[34]. Although the tip residues are in close proximity in the current model (~1.2 nm), the periplasmic crosslinking residues are separated by a distance >2.0 nm because of the PAS domain spacing. Thus, the transmembrane regions of Aer may undergo considerable motion within the arrays.

Distances indicative of higher-order structures with Aer were not observed in vitro because detergent solubilization breaks down TODs

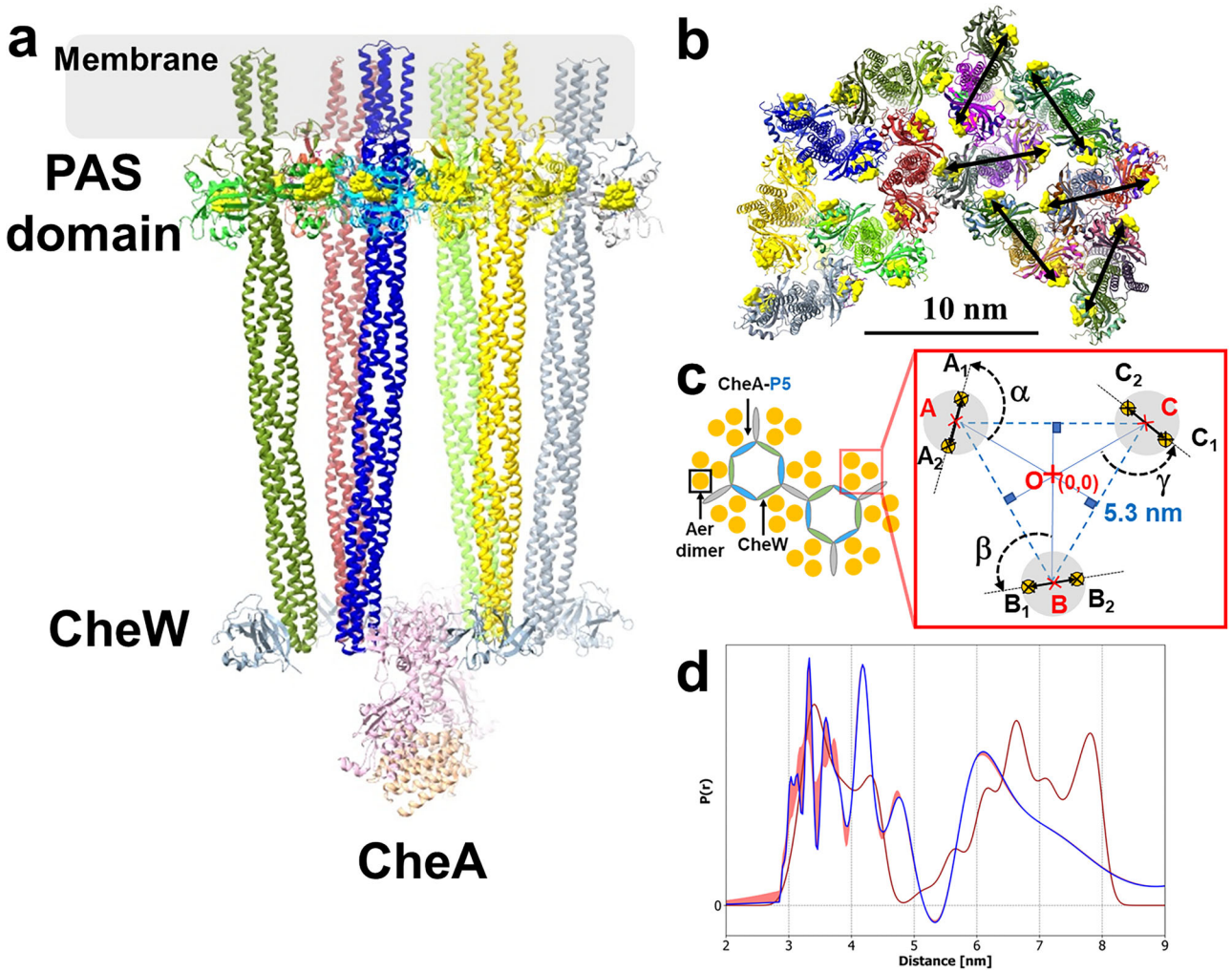

Fig. 5 | Aer forms higher-order structures *in cell*. **a** Model of a Aer/CheA/CheW core complex (2 trimer of dimers (TODs), 1 CheA dimer, 2 CheWs) as viewed parallel to the membrane, carried out with ChimeraX[120] (flavin cofactors represented as yellow surfaces). The figure is based on an Alphafold[121] reconstruction of an Aer/CheA/CheW homodimer. **b** Normal view from outside the membrane of four juxtaposed Aer TODs forming two core complexes. Black arrows represent the 4.1 nm separation between PAS subunits. **c** Schematic representing the larger organization of TODs within the hexagonal arrays. α,β,γ angles between 115° to 125° are required to assemble a TODs without the Per-Arnt-Sim (PAS) domains clashing (same designations as Fig. 1). In the inset, yellow dots with black crosses represent the FAD center in the PAS domain; two distance constraints are fixed: 4.1 nm separating the PAS domain in a homodimer (black arrows), and the 5.3 nm distance between dimer centers observed in a Tar/Tsr chemosensor array by cryo-ET[29]. The angles α, β, γ set four separations between FAD cofactors within a TODs (Supplementary Table 7). Blue squares represent right angles. **d** Comparison of a predicted distance distribution (brown curve) obtained from the homology model (Fig. 5b and Supplementary Table 8) and an experimental distance distribution obtained for Aer co-expressed with CheA/CheW in $^{2}H/^{15}N$ media (blue curve).

into homodimers, and it is very challenging to incorporate homogeneous, aligned TODs into nanodiscs in sufficient yields to carry out PDS. Furthermore, the extended structures of the arrays are more difficult to produce in vitro and have only been assembled with fragments of chemoreceptors[98,100–104]. Our results highlight the power of using isotopic labeling and *in cell* ESR to probe these large macromolecular complexes in their native environment.

iLOV as a flavoprotein probe for *in cell* ESR

To expand *in cell* ESR spectroscopy measurements to proteins lacking a native flavin cofactor, we used a small light-oxygen-voltage (LOV) sensing protein containing an FMN cofactor as a spin probe[105,106]. Our previous work had shown that LOV domains lacking the adduct-forming cysteine residue produce stable radicals upon photoreduction[105,107].

One of the major challenges for structural *in cell* studies involves the intracellular delivery of the spin probe[108]. First, the spin label or spin-labeled protein has to cross the outer membrane, cell wall and inner membrane, which is usually achieved with semi-destructive techniques such as electroporation, osmotic pressure or microinjection. If the spin label is delivered separately, it then must be specifically targeted to the protein of interest, a challenging endeavor. To overcome these issues, we genetically fused iLOV[106] (12.4 kDa) to the N-terminal P1 domain of the full-length histidine kinase CheA (75 kDa). CheA is composed of five domains, P1–P5 (Fig. 1c, d). The P1-domain contains the histidine residue that normally undergoes phosphorylation, the P2 domain constitutes the secondary messenger (CheY) binding site, the P3 domain dimerizes CheA, the P4 domain contains the ATP binding site, and the P5 domain interacts with the chemoreceptors (Aer/Tar) and CheW. The P1 and P2 domains of CheA are highly dynamic and are connected by flexible linkers (L1 and L2)[102]. Recent evidence suggests that the P1 domain of CheA may dimerize and associate with the core P3-P4-P5 domains in the inhibited off-state of the kinase when it is bound to chemoreceptors[30,98].

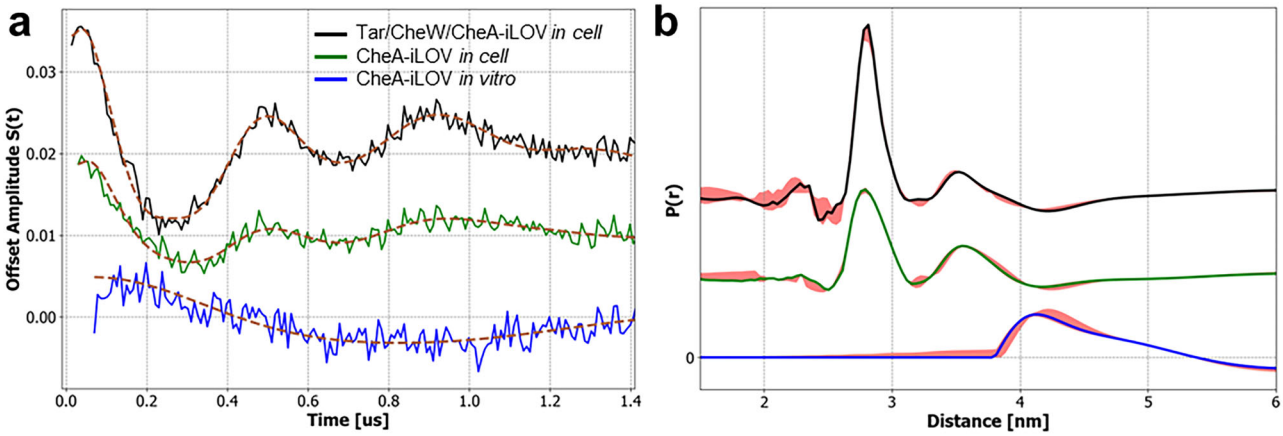

Fig. 6 | Four pulse double electron electron resonance (4P-DEER) measurements of CheA-iLOV in BL21 *E. coli* co-expressed with Tar and CheW (black curve), or alone (green curve), compared to purified CheA-iLOV in vitro (blue curve). a Time domain 4P-DEER and reconstructed time domain (SF-SVD method[117]) (dash brow line) measured at $T = 180$ K and (**b**) its associated domain distribution P(r). Errors in the distance distributions represented by red shading was calculated as described in Srivastava et al.[117].

First, we confirmed that the attachment of iLOV does not affect the autophosphorylation activity of CheA in vitro (Supplementary Fig. 10). Second, we generated an NSQ radical in iLOV by using blue light irradiation as previously characterized[109,110]. The concentration of the radical (Supplementary Table 9) was evaluated by cw-ESR, and the nature of the radical *in cell* was confirmed by pulsed ^{1}H-ENDOR spectroscopy (Supplementary Fig. 11). Third, we checked the viability of cells under blue light exposure (Supplementary Fig. 12). A decrease in colony-forming units (CFUs) with the irradiation time likely reflects iLOV acting as a photosensitizer to generate reactive oxygen species (ROS)[111]. *E. coli* cells were still active after 3 min of irradiation, although their viability was diminished. Fourth, we assessed the stability of the flavin radical in the cellular condition (Supplementary Fig. 13) by cw-ESR. The photogenerated radical was found to persist for hours with a half time $t_{1/2}$ ~ 5 h with a mono-exponential decay time constant $t_{decay} = 7.4 \pm 0.4$ h.

We then investigated the influence of the cell environment on the conformation of the P1 domain in CheA. The 4P-DEER spectrum (Fig. 6) of CheA-iLOV in solution revealed little or no dipolar signal; the weak, long-distance observed around 4–4.5 nm is likely an artefact due to the background subtraction. We then measured CheA-iLOV *in cell* at concentrations similar to those measured in vitro (Supplementary Table 9). In contrast to the in vitro sample, 4P-DEER experiments on CheA-iLOV either alone or co-expressed with CheW and Tar receptor indicated that the iLOV domains on the P1 domain of CheA reside close to each other, producing a dipolar interaction of 2.8 nm (which corresponds to an oscillation period of 420 ns) (Fig. 6).

The modulation depths for these experiments were relatively small ($\lambda = 4.3\%$ for Tar-CheW-CheA-iLOV *in cell* versus 1.3% and 0.4% for CheA-iLOV *in cell* and in vitro, respectively) (Supplementary Table 9). The comparison of CheA-iLOV in vitro to *in cell* indicates that the cellular environment alone favors some interaction of the CheA-P1 domains, perhaps due to molecular crowding in the cytoplasm. However, despite similar expression levels, when CheA-iLOV was co-expressed with its partners, the signal from the iLOV-iLOV interaction increased substantially.

Studies on Tar/CheA/CheW complexes indicate that association of CheA with CheW and receptors facilitates P1-P1 interactions, which would thereby bring the iLOV domains into close proximity of each other[98,102,112,113]. When bound to receptors, CheA may adopt different conformations associated with so-called kinase-on and kinase-off activity states[98,112,113]. Either or both of these states may involve P1 dimerization[98,112,113]. Efforts to alter the kinase activity state of CheA by adding the Tar attractant aspartate or repellant Ni^{2+} produced little difference in the distance domain (Supplementary Fig. 14), which could indicate that either the P1 domains remain dimerized regardless of activity state, or that ligand-induced shifts in the activity state involve a population of molecules that is too small to observe under these conditions.

Crystallographically characterized LOV dimers lacking N-cap or C-cap dimerization regions, including iLOV itself (PDB codes: 4NXB, 5A8B, 6WLE, 5DKL), produce flavin N5-to-N5 distances in the range of 2.3–2.6 nm. The longer 2.8 nm distance measured for CheA-iLOV *in cell* suggests that iLOV is not assuming one of these association states, and that rather the domains are being driven in proximity by P1-P1 interactions. The linker between iLOV and P1 provides considerable flexibility over 6-7 residues, and thus these measurements do not determine a specific mode of P1 association (e.g., parallel or anti-parallel). Nonetheless, the CheA-iLOV fusion successfully reported on the conformational state of CheA within receptor arrays and revealed domain arrangements that are difficult to recapitulate in reconstituted systems and are generally not assumed by the isolated kinase. Finally, the utility of iLOV as a fluorescence reporter provides an added benefit to this approach. Indeed, fusion to CheA does not alter the quantum yield of iLOV fluorescence, and the protein can be readily localized in *E. coli* cells by total internal reflection fluorescence (TIRF) microscopy (Supplementary Fig. 15b).

Effective methods to interrogate the structural and biophysical properties of proteins in their native cellular environments are in demand. Flavin cofactors, with their ability to stabilize radical states, have the potential to serve as genetically encodable probes for ESR spectroscopy. Here, we realize this concept by investigating the behavior of the FAD-binding aerotaxis receptor Aer in its native signaling assembly and by developing a small-flavoprotein probe iLOV that can be fused to any protein of interest. As Aer receptor conformations and oligomeric states are difficult to reproduce in vitro, *in cell* ESR spectroscopy provided insight into its assembly state with CheA and CheW. Q-band ^{1}H Davies ENDOR measurements revealed that Aer primarily forms an anionic semiquinone radical *in cell* with hfccs consistent with other ASQ-forming flavoproteins. This redox state has important implications for the Aer signaling mechanism and comments on the low potential of its membrane environment[28]. Q-Band 4P-DEER measurements revealed a flavin-flavin distance of 4.1 nm between Aer subunits within the homodimer, which agrees well

with previous in vitro measurements of isolated, chemically-reduced Aer[27]. In comparison to purified receptors, the *in cell* PDS measurements revealed additional distances consistent with chemoreceptor array formation in the cytoplasmic membrane. Additionally, temperature screening and isotopic labeling with ^{2}H and ^{15}N was performed to optimize relaxation properties for *in cell* PDS measurements, which enabled visualization of signaling complexes difficult to observe in vitro. Moreover, we extend the approach to a general target protein by incorporating a small flavin-containing domain, wherein stable radicals can be induced with light directly *in cell*. In particular, CheA-iLOV, when expressed in cells with its signaling partners, gave dipolar signals characteristic of domain associations that are not observed with purified samples, thereby demonstrating the importance of *in cell* measurement and the means to expand this method to a wide range of applications. Overall, this study should serve as a benchmark for future *in cell* investigations of flavoproteins.

Methods

Constructs and protein expression in *E. coli* BL21 (DE3)

Full-length *E. coli* Aer (1–506) and two Aer mutants (AerC193HC203H and AerY93HC193HC203H) were cloned into the pET-28a plasmid. Tar (1–553) was either cloned in pET-28a for the Tar/CheA/CheW construct or cloned into pCDF-DuetI for the Tar/CheW/CheA-iLOV construct. The histidine kinase CheA was cloned into the first multiple cloning site (MCS) of a pACYC-DuetI vector using the NcoI/BamHI restrictions sites, whereas the coupling protein CheW was cloned into the second MCS site of pACYC-DuetI using the NdeI/XhoI sites. *E. coli* BL21(DE3) were transformed by introducing pET-28a (Aer) and pACYC-DuetI (CheA/CheW). The cells were then selected on agar plates against 50 µg/mL of kanamycin A and 30 µg/mL of chloramphenicol.

CheA-iLOV was constructed by cutting the CheA/CheW coding sequence from the pACYC-DuetI vector with NcoI/XhoI and inserting it into pET-28a-iLOVf (Addgene plasmid # 63723) cut at the same restrictions sites to produce the fused CheA-iLOV in MCS-1 and CheW in MCS-II. *E. coli* BL21(DE3) were transformed by introducing pET-28a (CheA-iLOV/CheW) and pCDF-DuetI (Tar). The cells were then selected on agar plates against 50 µg/mL of kanamycin A and 50 µg/mL of streptomycin. CheA-iLOV expressed in BL21-DE3 cells were purified by nickel affinity and size exclusion chromatography on a preparative Superdex^{TM} 200 pg HiLoad 26/600 column (Supplementary Fig. 10).

Protein purification

Plated cells with corresponding plasmids fragment and antibiotics (Aer (pET-28a) with coexpression of CheA/CheW (pACYC) and CheA-iLOV (pET-28a)) were grown in 4 L LB at 37 °C for around 6 h and induced at an optical density at λ = 600 nm (OD_{600}) ~ 0.6 with 1 mM isopropyl β-D-1-thiogalactopyranoside (IPTG). The vials were then shaken overnight at 17 °C. The cell pellets were harvested by centrifugation at 2500 x *g* for 60 min at 4 °C. Cell pellets were resuspended in lysis buffer (50 mM Tris, 200 mM KCl, 10% glycerol, pH = 8.0) and were digested with 60 mg lysozyme and 0.1 mM PMSF for an hour at 4 °C. The Emulsiflex-C3 was equilibrated with lysis buffer and used to lyse the cell suspension at 15,000–18,000 psi in 3 passes.

Purification of Aer. As Aer is a membrane protein, an initial low-spin centrifugation of the cell lysate was carried out at 4000 x *g* for 20 min at 4 °C to remove cell debris. The low-spin supernatant was then ultracentrifuged at 100,000 x *g* for 1 h at 4 °C to acquire the insoluble fraction. The insoluble fraction was resuspended in lysis buffer at a 1:2 ratio, and the insoluble Aer protein was solubilized overnight at 4 °C with 1% Lauryl Maltose Neopentyl Glycol (Anatrace) (LMNG). The solubilized membrane fraction was centrifuged at 4000 x *g* for 10 min at 4 °C to remove any additional insoluble fraction. The supernatant was mixed with 0.1 mg/ml of FAD, then was gently rocked with 5 mL bed volume of lysis buffer prewashed Nickel NTA resin (Nickel NTA HTC Agarose Resin from GoldBio) overnight at 4 °C. The next morning, the resin was washed three times with lysis buffer containing 0.1% LMNG. The protein was then eluted from the resin with the elution buffer (50 mM Tris, pH = 8.0, 150 mM NaCl; 10% glycerol, 200 mM imidazole) and concentrated to the highest concentration possible with a 15 mL 50 kDa cutoff amicon filter and washed two times with the resuspension buffer (25 mM Tris, pH = 8.0, 150 mM NaCl; 10% glycerol, 1% LMNG). Aer protein was directly used for analysis after purification.

Purification of CheA-iLOV. The cell lysate was centrifugated at 30,000 x *g* for 45 min at 4 °C. The yellow supernatant was directly mixed with 5 mL bed volume of lysis buffer prewashed Nickel NTA resin (Nickel NTA HTC Agarose Resin from GoldBio) and left gently rocking overnight at 4 °C. The next morning, the resin was washed three times with lysis buffer. The protein was then eluted from the resin with the elution buffer (50 mM Tris, pH = 8.0, 150 mM NaCl; 10% glycerol, 200 mM imidazole) and concentrated to the highest concentration possible with a 15 mL 50 kDa cutoff Amicon filter. CheA-iLOV was stored at 4 °C for future analysis.

Viability assay of cells under irradiation

Aer/CheA/CheW and Tar/CheW/CheA-iLOV proteins were co-expressed in *E. coli* BL21(DE3) and induced with 1 mM IPTG at an OD_{600} around 0.6. Cells were harvested 3 h after induction at 37 °C and washed three times with PBS 1x buffer pH = 7.4, then concentrated to an OD_{600} equivalent to 100. 4 aliquots of 200 µL of cells were irradiated with a λ = 457 ± 10 nm blue LED (LZ1-00B202 from LedEngin) for 0 s, 3 s, 30 s and 180 s. 0.1 mL of cells were plated with sequential dilution ranging from OD_{600} = 1 to $OD_{600} = 1{\cdot}10^{-4}$. Agar plates were incubated overnight at 37 °C before counting the number of colony-forming units (CFUs) and determining the CFU/mL/OD_{600} value (Supplementary Fig. 12).

CheA autophosphorylation assays

CheA autophosphorylation was monitored by ^{32}P incorporation. All radioisotope assays were carried out in 5 mM Tris, pH = 7.5, 50 mM KCl, 10 mM $MgCl_2$, 0.5 mM DTT, 0.5 mM EDTA. Samples were prepared with 2 µM CheA and 4 µM CheW in a final volume of 25 µL. Following incubation for ~15 min, [γ–^{32}P]ATP was added to a final concentration of 1 mM and the reaction was quenched after 30 s using 4x SDS-PAGE loading buffer containing 50 mM EDTA at pH = 8.0. The samples were loaded onto a 4–20% Tris-glycine polyacrylamide protein gel purchased from Invitrogen. Gel electrophoresis was carried out for 35–60 min at 125 V constant voltage using a Tris-gly-SDS running buffer. The resulting gels were dried in a Bio-Rad Gel Dryer overnight and placed in a radiocassette for > 20 h prior to imaging on a Typhoon Image Scanner.

Preparation of *in cell* ESR samples

All the proteins were co-expressed with the appropriate antibiotic in *E. coli* BL21(DE3) cells under 1 mM IPTG induction. For the natural isotope experiments (^{1}H and ^{14}N), the cells were grown in autoclaved freshly prepared Luria broth media while the appropriate Celtone complete media (^{2}H, 97% or ^{15}N, 98% or ^{2}H, 97% and ^{15}N, 98%) from Cambridge Isotope Laboratory® was used for the isotope enriched experiments. Cells were grown in the appropriate media to an OD_{600} of ~ 0.5-0.6 and induced for 3 h at 37 °C (protonated media) or overnight (~16 h) at room temperature (deuterated media). The cells were then spun down, washed and resuspended in a small amount of 25% glycerol (25% d_3-glycerol in D_2O for the deuterated samples). The cells were then transferred into a ~1 mm I.D. capillary tube (Kimble® 71900-50 KIMAX® 50 µL precision microcapillaries) and spun down with a hematocrit centrifuge. Cell concentrations in the capillaries were determined by drying the samples at 150 °C, measuring the dry weight of cells and applying the following conversion factors[114]: 0.396 g/L DryWeight

(DW)/OD_{600} and OD_{600} of 1.0 ≡ $8{\cdot}10^8$ cells/ml (Supplementary Table 1). The spin concentration was determined by comparing the double integral value of the cw-ESR spectrum to a calibration curve based on similar measurements of Tempo (2,2,6,6-tetramethylpiperidine-1-oxyl) from 10 – 500 µM[115].

The CheA-iLOV protein was irradiated at room temperature with a λ = 457 ± 10 nm blue LED (LZ1-00B202 from LedEngin) for 3 min through the window of the ER 4123SHQE Bruker cavity to generate the semiquinone radical (see Supplementary Fig. 11 for the cw-ESR spectra). The X-band cw-ESR measurements were recorded at room temperature, and the samples were plunge frozen in liquid N_2 before carrying out the Q-band pulsed ESR measurements.

Cw-ESR oximetry experiments

Aer/CheA/CheW and Tar/CheW/CheA-iLOV proteins were co-expressed in *E. coli* BL21(DE3) and induced with 1 mM IPTG at an OD_{600} around 0.6. Cells were harvested during the log phase (3 h after induction at 37 °C) or during the stationary phase (3 h at 37 °C and 16 h at 22 °C). The cells were collected, washed three times with PBS 1x buffer, pH = 7.4, and concentrated to an OD_{600} = 100. A single crystal of lithium phtalocyanine was inserted into the capillary and then washed, and concentrated cells were added. cwESR spectrum were recorded with an amplitude modulation of either 0.01 G (with the presence of O_2 in the sample) or 0.001 G when depletion of oxygen became apparent (Supplementary Fig. 1). Peak-to-peak linewidth was measured by using a lorentzian fit function as described by Poole et al.[116].

Preparation of in vitro ESR samples

30 µM Aer purified protein stock solution (dissolved in 1% LMNG detergent) was supplemented with 25% glycerol and 10 mM DTT. 20 µL of this solution was quickly inserted into the ESR capillaries, and any oxygen was purged by 3 freeze-pump-thaw cycles with argon. The flame-sealed capillary was irradiated with λ = 457 ± 10 nm Blue LED (LZ1-00B202 from LedEngin) for 20 min. The irradiated sample was followed in situ by cw-ESR, and the sample was frozen just right after the maximum of intensity was generated (30 µM concentration in spin).

250 µM of CheA-iLOV purified protein stock solution was supplemented with 25% glycerol and 10 mM DTT. 20 µL of this solution was quickly inserted in the ESR capillaries, and any oxygen was purged by 3 freeze-pump-thaw cycles with argon. The flame-sealed capillary was irradiated with λ = 457 ± 10 nm Blue LED (LZ1-00B202 from LedEngin) during 20 min. The irradiated sample was followed in situ by cw-ESR, and the sample was frozen after the maximum of radical intensity was obtained (210 µM concentration in spin).

X-band cw-ESR

ESR spectra were recorded using a continuous wave X-band Bruker ElexSys E500 ESR spectrometer equipped with an ER 4123SHQE Bruker cavity. The acquisition parameters were fixed to 15 dB (6.325 mW) microwave power, 60 dB receiver gain, and 100 kHz modulation frequency. All cw-ESR spectra were recorded at 298 K with an amplitude modulation of 1 G to observe the hyperfine splitting. All of the simulations used to obtain the hyperfine coupling constants (hfccs) were carried out with EasySpin[90] (6.0.6) as implemented in MATLAB (R2021a; refer to code in the supplementary).

Q-Band pulsed ESR

The Q-band pulsed ESR analysis was carried out with an Elexsys E580 spectrometer equipped with a 10 W solid-state amplifier. All of the pulsed experiments were achieved in an EN 5107D2 Cavity, Q-Band ENDOR Pulsed ESR. A Bruker E-580 AWG Arbitrary Waveform Generator was used for the microwave pulse generation of the 4P-DEER, ENDOR and 3P-ESEEM sequences. Microwave pulses were generated by the Super-QFT-Upgrade Microwave Bridge for the relaxation time measurements. The temperature was varied by using an ER 4118HV-CF10-L FlexLine Cryogen-Free VT System. The pulse length (varying with the coupling range of the resonator and the microwave power used) was determined with a Rabi nutation measurement π-t_2-π/2-t-π-t-echo. All of the pulsed ESR experiments with Aer and iLOV *in cell* were conducted at temperatures of 150–180 K to maximize the phase memory time T_m, as assessed from the temperature profiles presented in Fig. 4b.

Time relaxation measurements. The resonator was critically coupled, and the magnetic field was chosen to be at the maximum peak signal intensity. The typical length of the microwave pulse was around 16 ns and 32 ns for a π/2 and π pulse, respectively, in these conditions.

The electron spin–lattice relaxation times T_1 were measured over the temperature range by an inversion recovery pulse sequence, π–t_2–π/2–t–π–t–echo by varying t_2. For each trace, 512 data points were collected with an appropriate time increment to ensure complete magnetization recovery. The trace was fitted by a bi-exponential model. The longer time decay T_{1L} was reported in the Supplementary Fig. 7. Phase-memory times T_m were measured over the temperature range by a two-pulse echo decay sequence, π/2–τ–π–τ–echo, while varying the time τ. The curves were fit by an exponential decay: $I(t) = I_0{*}\exp(-2\tau/T_m)$.

Pulsed ENDOR measurements. Pulsed Mims sequence π/2-tau-π/2-t_1-rf pulse-t_2-π/2-t-echo was employed to detect ^{2}H deuterium ENDOR signal. The π/2 pulses were chosen to be as short as possible and to be non-selective. To avoid the tau blind spot effect, the Mims ENDOR spectra were accumulated with a tau value varying from 120 ns to 150 ns. The different ^{2}H Mims spectra were summed over these tau values. The Davies sequence π-t_1-rf pulse-t_2-π/2-τ-π-τ-echo was employed for measuring ^{1}H proton signal, as the hfccs of some protons can be very large in the semiquinone radicals (10–30 MHz for some positions). The length of the selective microwave pulse was around 60 ns and 120 ns for a π/2 and π pulse, respectively.

For both sequences, (1) the resonator was critically coupled, (2) t_1 and t_2 were fixed to 1 µs to avoid any overlap between the microwave pulses and the radiofrequency (rf) pulse, and (3) a 20 µs radio-frequency (rf) pulse was applied with a 150 W Bruker RF amplifier.

4P-DEER measurements. 4-pulse DEER sequence π/2-t_1-π-t_1-π(pump)-t_2-π-t_2-echo was carried out at 150 K. The resonator was undercoupled to increase the microwave bandwidth. As a result, typical π/2 and π pulses of 18 ns and 36 ns were used. The time domain data was background subtracted, and distance distributions were obtained by the SF-SVD method[117]. Data processing of the SF-SVD-based method was used through the SVDReconstruction software (https://denoising.cornell.edu/). The distance domain was normalized (total probability fixed to 1). The Python scripts used for data treatments are available at https://github.com/TChauvire/.

Fluorescence Quantum Yield measurement

Purified CheA-iLOV was diluted in PBS 1x pH = 7.4 buffer with 10% glycerol to have a low level of absorbance at 420 nm and avoid any inner filter effect. UV-Visible absorption spectrum was recorded with an Agilent 8453 UV-Vis spectrophotometer (Supplementary Fig. 15a) with a 10 mm pathlength cuvette, and a A_{420} = 0.073 was determined. Fluorescence spectra were recorded with a spectrofluorimeter (Horiba Fluoromax Plus). The fluorescence quantum yield was determined by comparing the fluorescence spectrum of CheA-iLOV with the fluorescence spectra of two references: 5 µM (A_{420} = 0.024) and 10 µM (A_{420} = 0.047) of fluorescein diluted in 0.1 M NaOH. The formula used to calculate the quantum yield was[118,119]: $Q = Q_R \frac{F}{F_R} \frac{(1-10^{-A_R})}{(1-10^{-A})} \left(\frac{n^2}{n_R^2}\right)$ where Q is the

quantum yield, F is the integrated intensity, A is the absorbance measured at λ = 420 nm, n is the refractive index of the buffer, and the subscript R corresponds to the reference sample. A quantum yield Q_R(λ = 420 nm) value of 0.89 was used for the fluorescein.

In vivo fluorescence microscopy

Cells were cultured in LB media to an OD_{600} around 0.6 and induced for 3 h at 37 °C with 10 µM IPTG to express CheA-iLOV. After induction, the cells were pelleted by centrifugation, washed with phosphate buffer (10 mM K_2HPO_4, 10 mM KH_2PO_4, 0.1 mM EDTA, pH 7.0), and stored on ice until imaging. Imaging was performed using an inverted microscope (Leica DM-IRB, Wetzlar, Germany) equipped with TIRF (total internal reflection fluorescence) at 150 × magnification. The iLOV excitation wavelength was 488 nm, with a bandpass emission filter of 515 ± 20 nm. Raw images were processed further using ImageJ/FIJI (Supplementary Fig. 15b).

Reporting summary

Further information on research design is available in the Nature Portfolio Reporting Summary linked to this article.

Data availability

The raw and processed data generated in this study are deposited at the Github pages https://github.com/TChauvire and in the Zenodo database under accession code https://doi.org/10.5281/zenodo.15353349. Crystallographic data of LOV dimers that are mentioned in the Results and Discussion section are accessible with the PDB codes: 4NXB, 5A8B, 6WLE, and 5DKL. Source data file with raw numbers for charts and graphs are provided with this paper. Source data are provided in this paper.

Code availability

Codes are available at the Github pages https://github.com/TChauvire/ or in the Zenodo database under accession code https://doi.org/10.5281/zenodo.15353349.

References

1. Fraaije, M. W. & Mattevi, A. Flavoenzymes: Diverse catalysts with recurrent features. *Trends Biochem. Sci.* **25**, 126–132 (2000).
2. Conrad, K. S., Manahan, C. C. & Crane, B. R. Photochemistry of flavoprotein light sensors. *Nat. Chem. Biol.* **10**, 801–809 (2014).
3. Glantz, S. T. et al. Functional and topological diversity of LOV domain photoreceptors. *Proc. Natl. Acad. Sci. USA* **113**, E1442–E1451 (2016).
4. Mattevi, A. To be or not to be an oxidase: challenging the oxygen reactivity of flavoenzymes. *Trends Biochem. Sci.* **31**, 276–283 (2006).
5. Moreno, A. et al. Cofactors and pathogens: flavin mononucleotide and flavin adenine dinucleotide (FAD) biosynthesis by the FAD synthase from Brucella ovis. *IUBMB Life* **74**, 655–671 (2022).
6. Pimviriyakul, P. & Chaiyen, P. *Overview of Flavin-Dependent Enzymes*. *Enzymes* **47**, 1–36 (2020).
7. Losi, A. & Gärtner, W. Solving blue light riddles: New lessons from flavin-binding LOV photoreceptors. *Photochem. Photobiol.* **93**, 141–158 (2017).
8. Herrou, J. & Crosson, S. Function, structure and mechanism of bacterial photosensory LOV proteins. *Nat. Rev. Microbiol.* **9**, 713–723 (2011).
9. Romero, E., Gómez Castellanos, J. R., Gadda, G., Fraaije, M. W. & Mattevi, A. Same substrate, many reactions: oxygen activation in flavoenzymes. *Chem. Rev.* **118**, 1742–1769 (2018).
10. Pritchett, D. & Reddy, A. B. No FAD, no CRY: redox and circadian rhythms. *Trends Biochem. Sci.* **42**, 497–499 (2017).
11. Tuz, K. et al. Identification of the riboflavin cofactor-binding site in the Vibrio cholerae ion-pumping NQR complex: A novel structural motif in redox enzymes. *J. Biol. Chem.* **298**, 102182 (2022).
12. Edwards, A. M., Weber, S. & Schleicher, E. Structure and general properties of flavins. *Methods in Mol. Biol.* **1146**, 3–13 (2014).
13. Nohr, D., Weber, S. & Schleicher, E. EPR spectroscopy on flavin radicals in flavoproteins. *Methods Enzymol.* **620**, 251–275 (2019).
14. Brosi, R., Bittl, R. & Engelhard, C. EPR on flavoproteins. *Methods in Mol. Biol.* **1146**, 341–360 (2014).
15. Rostas, A. et al. Long-Lived Hydrated FMN Radicals: EPR characterization and implications for catalytic variability in flavoproteins. *J. Am. Chem. Soc.* **140**, 16521–16527 (2018).
16. Okafuji, A., Schnegg, A., Schleicher, E., Möbius, K. & Weber, S. G-tensors of the flavin adenine dinucleotide radicals in glucose oxidase: A comparative multifrequency electron paramagnetic resonance and electron-nuclear double resonance. *J. Phys. Chem. B* **112**, 3568–3574 (2008).
17. Chandrasekaran, S. et al. Tuning flavin environment to detect and control light-induced conformational switching in Drosophila cryptochrome. *Commun. Biol.* **4**, 249 (2021).
18. Schleicher, E. et al. The electronic state of flavoproteins: investigations with proton electron-nuclear double resonance. *Appl. Magn. Reson.* **37**, 339–352 (2010).
19. Martínez, J. I., Alonso, P. J., Gómez-Moreno, C. & Medina, M. One- and two-dimensional ESEEM spectroscopy of flavoproteins. *Biochemistry* **36**, 15526–15537 (1997).
20. Bollen, Y. J. M., Westphal, A. H., Lindhoud, S., Van Berkel, W. J. H. & Van Mierlo, C. P. M. Distant residues mediate picomolar binding affinity of a protein cofactor. *Nat. Commun.* **3**, 1010 (2012).
21. Krauss, U. et al. Distribution and phylogeny of light-oxygen-voltage-blue-light-signaling proteins in the three kingdoms of life. *J. Bacteriol.* **191**, 7234–7242 (2009).
22. Taylor, B. L., Watts, K. J. & Johnson, M. S. Oxygen and redox sensing by two-component systems that regulate behavioral responses: behavioral assays and structural studies of aer using in vivo disulfide cross-linking. *Methods in Enzymol.* **422** 190–232 (2007).
23. Taylor, B. L. Aer on the inside looking out: Paradigm for a PAS-HAMP role in sensing oxygen, redox and energy. *Mol. Microbiol.* **65**, 1415–1424 (2007).
24. Taylor, B. L., Rebbapragada, A. & Johnson, M. S. The FAD-PAS domain as a sensor for behavioral responses in Escherichia coli. *Antioxid. Redox Signal.* **3**, 867–879 (2001).
25. Taylor, B. L., Zhulin, I. B. & Johnson, M. S. Aerotaxis and other energy-sensing behavior in bacteria. *Annu. Rev. Microbiol.* **53**, 103–128 (1999).
26. Taylor, B. & Zhulin, I. PAS domains: internal sensors of oxygen, redox potential, and light. *Microbiol. Mol. Biol. Rev.* **63**, 479–506 (1999).
27. Samanta, D., Widom, J., Borbat, P. P., Freed, J. H. & Crane, B. R. Bacterial energy sensor Aer modulates the activity of the chemotaxis kinase CheA based on the redox state of the flavin cofactor. *J. Biol. Chem.* **291**, 25809–25814 (2016).
28. Maschmann, Z. A., Chua, T. K., Chandrasekaran, S., Ibáñez, H. & Crane, B. R. Redox properties and PAS domain structure of the Escherichia coli energy sensor Aer indicate a multistate sensing mechanism. *J. Biol. Chemi.* **298**, 102598 (2022).
29. Burt, A. et al. Complete structure of the chemosensory array core signalling unit in an E. coli minicell strain. *Nat. Commun.* **11**, 743 (2020).
30. Muok, A. R., Briegel, A. & Crane, B. R. Regulation of the chemotaxis histidine kinase CheA: A structural perspective.*Biochim. Biophys. Acta Biomembr.* **1862**, 183030 (2019).

31. Briegel, A. et al. Structure of bacterial cytoplasmic chemoreceptor arrays and implications for chemotactic signaling. *ELife* **3**, e02151 (2014).
32. Briegel, A. et al. Bacterial chemoreceptor arrays are hexagonally packed trimers of receptor dimers networked by rings of kinase and coupling proteins. *Proc. Natl Acad. Sci. USA* **109**, 3766–3771 (2012).
33. Liu, J. et al. Molecular architecture of chemoreceptor arrays revealed by cryoelectron tomography of Escherichia coli minicells. *Proc. Natl Acad. Sci. USA* **109**, E1481–E1488 (2012).
34. Amin Divya, N., Taylor Barry, L. & Johnson Mark, S. Organization of the aerotaxis receptor Aer in the membrane of Escherichia coli. *J. Bacteriol.* **189**, 7206–7212 (2007).
35. Engelhard, C. et al. Cellular metabolites enhance the light sensitivity of Arabidopsis cryptochrome through alternate electron transfer pathways. *Plant Cell* **26**, 4519–4531 (2014).
36. Herbel, V. et al. Lifetimes of Arabidopsis cryptochrome signaling states in vivo. *Plant J.* **74**, 583–592 (2013).
37. Burney, S. et al. Single amino acid substitution reveals latent photolyase activity in Arabidopsis cry1. *Angew. Chem. Int. Ed.* **51**, 9356–9360 (2012).
38. Bouly, J.-P. et al. Cryptochrome blue light photoreceptors are activated through interconversion of flavin redox states*. *J. Biol. Chem.* **282**, 9383–9391 (2007).
39. Banerjee, R. et al. The signaling state of arabidopsis cryptochrome 2 contains flavin semiquinone*. *J. Biol. Chem.* **282**, 14916–14922 (2007).
40. Hoang, N. et al. Human and Drosophila cryptochromes are light activated by flavin photoreduction in living cells. *PLoS Biol.* **6**, 1559–1569 (2008).
41. Ben-Ishay, Y. et al. Exploring the dynamics and structure of PpiB in living Escherichia coli cells using electron paramagnetic resonance spectroscopy. *Protein Sci.* **33**, e4903 (2024).
42. Haysom, S. F. et al. Darobactin B stabilises a lateral-closed conformation of the BAM complex in E. coli cells. *Angew. Chem. Int. Ed.* **62**, e202218783 (2023).
43. Jana, S. et al. Ultrafast bioorthogonal spin-labeling and distance measurements in mammalian cells using small, genetically encoded tetrazine amino acids. *J. Am. Chem. Soc.* **145**, 14608–14620 (2023).
44. Pierro, A. et al. In-cell investigation of the conformational landscape of the GTPase UreG by SDSL-EPR. *iScience* **26**, 107855 (2023).
45. Pierro, A. et al. Probing the structural dynamics of a bacterial chaperone in its native environment by nitroxide-based EPR spectroscopy. *Chem. A Eur. J.* **28**, e202202249 (2022).
46. Torricella, F., Barbieri, L., Bazzurro, V., Diaspro, A. & Banci, L. Protein delivery to living cells by thermal stimulation for biophysical investigation. *Sci. Rep.* **12**, 17190 (2022).
47. Collauto, A. et al. Compaction of RNA duplexes in the cell. *Angew. Chem. Int. Ed.* **59**, 23025–23029 (2020).
48. Widder, P., Schuck, J., Summerer, D. & Drescher, M. Combining site-directed spin labeling in vivo and in-cell EPR distance determination. *Phys. Chem. Chem. Phys.* **22**, 4875–4879 (2020).
49. Seal, M. et al. GdIII-19F Distance measurements for proteins in cells by electron-nuclear double resonance. *Angew. Chem. Int. Ed.* **62**, e202218780 (2023).
50. Kucher, S., Elsner, C., Safonova, M., Maffini, S. & Bordignon, E. In-cell double electron–electron resonance at nanomolar protein concentrations. *J. Phys. Chem. Lett.* **12**, 3679–3684 (2021).
51. Miao, Q. et al. A two-armed probe for in-cell deer measurements on proteins**. *Chem. A Eur. J.* **26**, 17128–17133 (2020).
52. Kucher, S., Korneev, S., Klare, J. P., Klose, D. & Steinhoff, H.-J. In cell Gd3+-based site-directed spin labeling and EPR spectroscopy of eGFP. *Phys. Chem. Chem. Phys.* **22**, 13358–13362 (2020).
53. Yang, Y. et al. In-cell destabilization of a homodimeric protein complex detected by DEER spectroscopy. *Proc. Natl. Acad. Sci. USA* **117**, 20566–20575 (2020).
54. Yang, Y., Yang, F., Li, X.-Y., Su, X.-C. & Goldfarb, D. In-cell epr distance measurements on ubiquitin labeled with a rigid PyMTA-Gd(III) tag. *J. Phys. Chem. B* **123**, 1050–1059 (2019).
55. Armstrong, Z. et al. Recent applications of triarylmethyl (TAM) derivatives as electron paramagnetic resonance (EPR) spin labels in biomacromolecular structural studies. *Appl. Magn. Reson.* **55**, 29–44 (2024).
56. Hasanbasri, Z., Singewald, K., Gluth, T. D., Driesschaert, B. & Saxena, S. Cleavage-resistant protein labeling with hydrophilic trityl enables distance measurements in-cell. *J. Phys. Chem. B* **125**, 5265–5274 (2021).
57. Yang, Y. et al. In-cell trityl–trityl distance measurements on proteins. *J. Phys. Chem. Lett.* **11**, 1141–1147 (2020).
58. Fleck, N. et al. SLIM: a short-linked, highly redox-stable trityl label for high-sensitivity in-cell EPR distance measurements. *Angew. Chem. Int. Ed.* **59**, 9767–9772 (2020).
59. Meichsner, S. L., Kutin, Y. & Kasanmascheff, M. In-Cell Characterization of the stable tyrosyl radical in E. coli ribonucleotide reductase using advanced EPR spectroscopy. *Angew. Chem. Int. Ed.* **60**, 19155–19161 (2021).
60. Meron, S. et al. Tracking disordered extracellular domains of membrane proteins in the cell with Cu(II)-based spin labels. *J. Phys. Chem. B* **128**, 8908–8914 (2024).
61. Shenberger, Y., Gevorkyan-Airapetov, L., Hirsch, M., Hofmann, L. & Ruthstein, S. An in-cell spin-labelling methodology provides structural information on cytoplasmic proteins in bacteria. *Chem. Commun.* **59**, 10524–10527 (2023).
62. Garcia, D., Watts, K. J., Johnson, M. S. & Taylor, B. L. Delineating PAS-HAMP interaction surfaces and signalling-associated changes in the aerotaxis receptor Aer. *Mol. Microbiol.* **100**, 156–172 (2016).
63. Kim, S. H., Wang, W. & Kim, K. K. Dynamic and clustering model of bacterial chemotaxis receptors: structural basis for signaling and high sensitivity. *Proc. Natl. Acad. Sci. USA* **99**, 11611–11615 (2002).
64. Volkmer, B. & Heinemann, M. Condition-dependent cell volume and concentration of escherichia coli to facilitate data conversion for systems biology modeling. *PLOS ONE* **6**, e23126 (2011).
65. Liu, K. J. et al. Lithium phthalocyanine: a probe for electron paramagnetic resonance oximetry in viable biological systems. *Proc. Natl. Acad. Sci. USA* **90**, 5438–5442 (1993).
66. Ahmad, R. & Kuppusamy, P. Theory, instrumentation, and applications of electron paramagnetic resonance oximetry. *Chem. Rev.* **110**, 3212–3236 (2010).
67. Teucher, M. et al. A new perspective on membrane-embedded Bax oligomers using DEER and bioresistant orthogonal spin labels. *Sci. Rep.* **9**, 13013 (2019).
68. Pouvreau, S. Genetically encoded reactive oxygen species (ROS) and redox indicators. *Biotechnol. J.* **9**, 282–293 (2014).
69. Salinas, G., Pellizza, L., Margenat, M., Fló, M. & Fernández, C. Tuned Escherichia coli as a host for the expression of disulfide-rich proteins. *Biotechnol. J.* **6**, 686–699 (2011).
70. Kostyuk, A. I., Panova, A. S., Bilan, D. S. & Belousov, V. V. Redox biosensors in a context of multiparameter imaging. *Free Radic. Biol. Med.* **128**, 23–39 (2018).
71. Pettersen, V. K., Steinsland, H. & Wiker, H. G. Comparative proteomics of enterotoxigenic Escherichia coli reveals differences in surface protein production and similarities in metabolism. *J. Proteome Res.* **17**, 325–336 (2018).
72. Li, M. & Hazelbauer, G. L. Cellular stoichiometry of the components of the chemotaxis signaling complex. *J. Bacteriol.* **186**, 3687–3694 (2004).

73. Bibikov, S. I., Barnes, L. A., Gitin, Y. & Parkinson, J. S. Domain organization and flavin adenine dinucleotide-binding determinants in the aerotaxis signal transducer Aer of Escherichia coli. *Proc. Natl. Acad. Sci. USA* **97**, 5830–5835 (2000).
74. Bibikov, S. I., Biran, R., Rudd, K. E. & Parkinson, J. S. A signal transducer for aerotaxis in Escherichia coli. *J. Bacteriol.* **179**, 4075–4079 (1997).
75. Massey, V. The reactivity of oxygen with flavoproteins. *Int. Congr. Ser.* **1233**, 3–11 (2002).
76. Penzer, G. R. The chemistry of flavins and flavoproteins. Aerobic photochemistry. *Biochem. J.* **116**, 733–743 (1970).
77. Campbell, A. J., Watts, K. J., Johnson, M. S. & Taylor, B. L. Gain-of-function mutations cluster in distinct regions associated with the signalling pathway in the PAS domain of the aerotaxis receptor, Aer. *Mol. Microbiol.* **77**, 575–586 (2010).
78. Watts, K. J., Johnson, M. S. & Taylor, B. L. Minimal requirements for oxygen sensing by the aerotaxis receptor Aer. *Mol. Microbiol.* **59**, 1317–1326 (2006).
79. Schiemann, O. et al. Benchmark test and guidelines for DEER/PELDOR experiments on nitroxide-labeled biomolecules. *J. Am. Chem. Soc.* **143**, 17875–17890 (2021).
80. Borbat, P. P. & Freed, J. H. Dipolar spectroscopy – single-resonance methods. *eMagRes.* **6**, 465–494 (2017).
81. Jeschke, G. Dipolar spectroscopy – double-resonance methods. in *eMagRes*. **5**, 1459–1476 (2016).
82. Schmidt, T., Ghirlando, R., Baber, J. & Clore, G. M. Quantitative resolution of monomer-dimer populations by inversion modulated DEER EPR spectroscopy. *ChemPhysChem* **17**, 2987–2991 (2016).
83. Georgieva, E. R., Borbat, P. P., Norman, H. D. & Freed, J. H. Mechanism of influenza a M2 transmembrane domain assembly in lipid membranes. *Sci. Rep.* **5**, 11757 (2015).
84. Upadhyay, A. K., Borbat, P. P., Wang, J., Freed, J. H. & Edmondson, D. E. Determination of the oligomeric states of human and rat monoamine oxidases in the outer mitochondrial membrane and octyl β-d-glucopyranoside micelles using pulsed dipolar electron spin resonance spectroscopy. *Biochemistry* **47**, 1554–1566 (2008).
85. Lindgren, M. et al. Electron spin echo decay as a probe of aminoxyl environment in spin-labeled mutants of human carbonic anhydrase II. *J. Chem. Soc. Perkin Trans.* **2**, 2549–2554 (1997).
86. Huber, M. et al. Phase memory relaxation times of spin labels in human carbonic anhydrase II: Pulsed EPR to determine spin label location. *Biophys. Chem.* **94**, 245–256 (2001).
87. El Mkami, H., Ward, R., Bowman, A., Owen-Hughes, T. & Norman, D. G. The spatial effect of protein deuteration on nitroxide spin-label relaxation: Implications for EPR distance measurement. *J. Magn. Reson.* **248**, 36–41 (2014).
88. Gilbert, B. C., Davies, M. J., Murphy, D. M., Kay, C. W. M. & Weber, S. EPR of Radical Intermediates in Flavoenzymes. in *Electron Paramagnetic Resonance* 180 (The Royal Society of Chemistry, 2002).
89. Schleicher, E., Bittl, R. & Weber, S. New roles of flavoproteins in molecular cell biology: Blue-light active flavoproteins studied by electron paramagnetic resonance. *FEBS J.* **276**, 4290–4303 (2009).
90. Stoll, S. & Schweiger, A. EasySpin, a comprehensive software package for spectral simulation and analysis in EPR. *J. Magn. Reson.* **178**, 42–55 (2006).
91. Barquera, B. et al. X- and W-band EPR and Q-band ENDOR studies of the flavin radical in the Na+-translocating NADH:quinone oxidoreductase from Vibrio cholerae. *J. Am. Chem. Soc.* **125**, 265–275 (2003).
92. Leniart, D. S., Connor, H. D. & Freed, J. H. An ESR and ENDOR study of spin relaxation of semiquinones in liquid solution. *J. Chem. Phys.* **63**, 165–199 (1975).
93. Kathirvelu, V., Sato, H., Eaton, S. S. & Eaton, G. R. Electron spin relaxation rates for semiquinones between 25 and 295 K in glass-forming solvents. *J. Magn. Reson.* **198**, 111–120 (2009).
94. Goslar, J., Hoffmann, S. K. & Lijewski, S. Dynamics of 4-oxo-TEMPO-d16-15N nitroxide-propylene glycol system studied by ESR and ESE in liquid and glassy state in temperature range 10-295 K. *J. Magn. Reson.* **269**, 162–175 (2016).
95. Zecevic, A., Eaton, G. R., Eaton, S. S. & Lindgren, M. Dephasing of electron spin echoes for nitroxyl radicals in glassy solvents by non-methyl and methyl protons. *Mol. Phys.* **95**, 1255–1263 (1998).
96. Nakagawa, K., Candelaria, M. B., Chik, W. W. C., Eaton, S. S. & Eaton, G. R. Electron-spin relaxation times of chromium(V). *J. Magn. Reson* **98**, 81–91 (1992).
97. Eaton, S. S. & Eaton, G. R. Relaxation times of organic radicals and transition metal Ions. in *Distance Measurements in Biological Systems by EPR* 29–154 (Springer US, Boston, MA, 2000).
98. Muok, A. R. et al. Engineered chemotaxis core signaling units indicate a constrained kinase-off state. *Sci. Signal.* **13**, eabc1328 (2020).
99. Li, M. & Hazelbauer, G. L. Core unit of chemotaxis signaling complexes. *Proc. Natl. Acad. Sci. USA* **108**, 9390–9395 (2011).
100. Li, X., Eyles, S. J. & Thompson, L. K. Hydrogen exchange of chemoreceptors in functional complexes suggests protein stabilization mediates long-range allosteric coupling. *J. Biol. Chem.* **294**, 16062–16079 (2019).
101. Haglin, E. R., Yang, W., Briegel, A. & Thompson, L. K. His-tag-mediated dimerization of chemoreceptors leads to assembly of functional nanoarrays. *Biochemistry* **56**, 5874–5885 (2017).
102. Greenswag, A. R. et al. Preformed soluble chemoreceptor trimers that mimic cellular assembly states and activate CheA autophosphorylation. *Biochemistry* **54**, 3454–3468 (2015).
103. Wolanin, P. M. et al. Self-assembly of receptor/signaling complexes in bacterial chemotaxis. *Proc. Natl. Acad. Sci. USA* **103**, 14313–14318 (2006).
104. Shrout, A. L., Montefusco, D. J. & Weis, R. M. Template-directed assembly of receptor signaling complexes. *Biochemistry* **42**, 13379–13385 (2003).
105. Yee, E. F. et al. Signal transduction in light–oxygen–voltage receptors lacking the adduct-forming cysteine residue. *Nat. Commun.* **6**, 10079 (2015).
106. Chapman, S. et al. The photoreversible fluorescent protein iLOV outperforms GFP as a reporter of plant virus infection. *Proc. Natl. Acad. Sci. USA* **105**, 20038–20043 (2008).
107. Yee, E. F. et al. Peripheral methionine residues impact flavin photoreduction and protonation in an engineered lov domain light sensor. *Biochemistry* **60**, 1148–1164 (2021).
108. Pierro, A. & Drescher, M. Dance with spins: site-directed spin labeling coupled to electron paramagnetic resonance spectroscopy directly inside cells. *Chem. Commun.* **59**, 1274–1284 (2023).
109. Dunleavy, R., Chandrasekaran, S. & Crane, B. R. Enzymatic spin-labeling of protein n- and c-termini for electron paramagnetic resonance spectroscopy. *Bioconjug. Chem.* **34**, 686–695 (2023).
110. Kopka, B. et al. Electron transfer pathways in a light, oxygen, voltage (LOV) protein devoid of the photoactive cysteine. *Sci. Rep.* **7**, 13346 (2017).
111. Endres, S. et al. An optogenetic toolbox of LOV-based photosensitizers for light-driven killing of bacteria. *Sci. Rep.* **8**, 15021 (2018).
112. Cassidy, C. K. et al. Structure of the native chemotaxis core signaling unit from phage E-protein lysed E. coli cells. *mBio* **14**, e00793–23 (2023).
113. Tran, T., Karunanayake Mudiyanselage, A. P. K. K., Eyles, S. J. & Thompson, L. K. Bacterial chemoreceptor signaling complexes

control kinase activity by stabilizing the catalytic domain of CheA. *Proc. Natl. Acad. Sci.* **120**, e2218467120 (2023).
114. Myers, J. A., Curtis, B. S. & Curtis, W. R. Improving accuracy of cell and chromophore concentration measurements using optical density. *BMC Biophys.* **6**, 4 (2013).
115. Lund, A., Shiotani, M. & Shimada, S. in *Principles and Applications of ESR Spectroscopy* (eds. Lund, A., Shiotani, M. & Shimada, S.) 409–438 (Springer Netherlands, Dordrecht, 2011).
116. Poole, C. P. & Farach, H. A. Line shapes in electron spin resonance. *Bull. Magn. Reson* **1**, 162–194 (1979).
117. Srivastava, M. & Freed, J. H. Singular value decomposition method to determine distance distributions in pulsed dipolar electron spin resonance: II. estimating uncertainty. *J. Phys. Chem. A* **123**, 359–370 (2019).
118. Lakowicz, J. R. in *Principles of Fluorescence Spectroscopy* (ed. Lakowicz, J. R.) 27–61 (Springer US, Boston, MA, 2006).
119. Würth, C., Grabolle, M., Pauli, J., Spieles, M. & Resch-Genger, U. Relative and absolute determination of fluorescence quantum yields of transparent samples. *Nat. Protoc.* **8**, 1535–1550 (2013).
120. Pettersen, E. F. et al. UCSF Chimera—A visualization system for exploratory research and analysis. *J. Comput. Chem.* **25**, 1605–1612 (2004).
121. Jumper, J. et al. Highly accurate protein structure prediction with AlphaFold. *Nature* **596**, 583–589 (2021).

Acknowledgements

We thank Curt R. Dunnam and Walt P. Ford for the assistance and the repairs of the pulsed ESR spectrometer, Dr. Zachary Maschmann for the preparation and the expression of Aer site-directed variants, and Dr. Madhur Srivastava for the help with the use of the SF-SVD software. We thank Dr. Boris Dzikovsky for the synthesis of LiPc crystal for the oximetry measurements. We acknowledge Dr. Nirmalya Bag and the Baird lab for their help with the TIRF microscopy experiments. This work was supported by grants from the National Science Foundation: MCB 2129729 to B.R.C.; National Institutes of Health: R35GM122535 to B.R.C. and R35GM148272 to J.H.F.; and by the National Institute Of General Medical Sciences (NIGMS) of the National Institutes of Health (NIH) under Award Number R24GM146107 and P41GM103521 to J.H.F. and B.R.C.

Author contributions

S.C., T.C., R.D., and B.R.C. conceived of and designed the research. B.R.C. supervised the project. T.C., S.C., and R.D. designed and carried out the experiments. T.C., S.C., R.D., J.H.F., and B.R.C. analyzed the data. T.C., S.C., and B.R.C. wrote the manuscript; all authors revised and commented on the manuscript.

Competing interests

The authors declare no competing interests.

Additional information

Supplementary information The online version contains supplementary material available at https://doi.org/10.1038/s41467-025-60623-6.

Correspondence and requests for materials should be addressed to Brian R. Crane.

Peer review information *Nature Communications* thanks Glenn Millhauser, Kylie Watts, and the other anonymous reviewer(s) for their contribution to the peer review of this work. A peer review file is available.